Atmos. Meas. Tech. Discuss., 8, 10983–11028, 2015
www.atmos-meas-tech-discuss.net/8/10983/2015/
doi:10.5194/amtd-8-10983-2015

Atmospheric Measurement Techniques Discussions
Open Access

Optimization of a gas sampling system for measuring eddy-covariance fluxes of H_2O and CO_2

S. Metzger[1,2], G. Burba[3], S. P. Burns[4,5], P. D. Blanken[4], J. Li[3], H. Luo[1,2], and R. C. Zulueta[1]

[1]National Ecological Observatory Network, Fundamental Instrument Unit, Boulder, Colorado, USA
[2]University of Colorado, Institute for Arctic and Alpine Research, Boulder, Colorado, USA
[3]LI-COR Biosciences, Environmental Division, Lincoln, Nebraska, USA
[4]University of Colorado, Department of Geography, Boulder, Colorado, USA
[5]National Center for Atmospheric Research, Mesoscale and Microscale Meteorology Laboratory, Boulder, Colorado, USA

Received: 16 July 2015 – Accepted: 22 September 2015 – Published: 26 October 2015

Correspondence to: S. Metzger (smetzger@neoninc.org)

Published by Copernicus Publications on behalf of the European Geosciences Union.

Abstract

Several initiatives are currently emerging to observe the exchange of energy and matter between the earth's surface and atmosphere standardized over larger space and time domains. For example, the National Ecological Observatory Network (NEON) and the Integrated Carbon Observing System (ICOS) will provide the ability of unbiased ecological inference across eco-climatic zones and decades by deploying highly scalable and robust instruments and data processing. In the construction of these observatories, enclosed infrared gas analysers are widely employed for eddy-covariance applications. While these sensors represent a substantial improvement compared to their open- and closed-path predecessors, remaining high-frequency attenuation varies with site properties, and requires correction. Here, we show that the gas sampling system substantially contributes to high-frequency attenuation, which can be minimized by careful design. From laboratory tests we determine the frequency at which signal attenuation reaches 50 % for individual parts of the gas sampling system. For different models of rain caps and particulate filters, this frequency falls into ranges of 2.5–16.5 Hz for CO_2, 2.4–14.3 Hz for H_2O, and 8.3–21.8 Hz for CO_2, 1.4–19.9 Hz for H_2O, respectively. A short and thin stainless steel intake tube was found to not limit frequency response, with 50 % attenuation occurring at frequencies well above 10 Hz for both H_2O and CO_2. From field tests we found that heating the intake tube and particulate filter continuously with 4 W was effective, and reduced the occurrence of problematic relative humidity levels (RH > 60 %) by 50 % in the infrared gas analyser cell. No further improvement of H_2O frequency response was found for heating in excess of 4 W. These laboratory and field tests were reconciled using resistor-capacitor theory, and NEON's final gas sampling system was developed on this basis. The design consists of the stainless steel intake tube, a pleated mesh particulate filter, and a low-volume rain cap in combination with 4 W of heating and insulation. In comparison to the original design, this reduced the high-frequency attenuation for H_2O by $\approx 3/4$, and the remaining cospectral correction did not exceed 3 %, even at a very high relative humidity (95 %). This

AMTD

8, 10983–11028, 2015

Optimization of a gas sampling system for measuring eddy-covariance fluxes

S. Metzger et al.

standardized design can be used across a wide range of eco-climates and site layouts, and maximizes practicability due to minimal flow resistance and maintenance needs. Furthermore, due to minimal high-frequency spectral loss, it supports the routine application of adaptive correction procedures, and enables more automated data processing across sites.

1 Introduction

The ecological research community long ago identified the need for integrated research programs that focus on understanding the underlying ecological processes and the impacts on biological diversity due to global change (Lubchenco et al., 1991). The need for a research infrastructure that would span both temporal and spatial scales from regional- to continental-scale was re-emphasized when the National Research Council issued the "Grand Challenges of Environmental Science" (National Research Council, 2001). Several large research infrastructure projects have been designed and initiated to address these challenges including the US National Ecological Observatory Network (NEON), Europe's Integrated Carbon Observation System (ICOS), and Australia's Terrestrial Ecosystem Research Network (TERN).

NEON has adopted a requirements-based approach to guide its science and infrastructure design. Such approach decomposes the overarching science goals (e.g. Grand Challenges) into a hierarchy of objective design statements (Schimel et al., 2011). Those design statements capture the scope of the system, as well as how it will perform. Combined with input from the scientific community they also serve as the specification for selecting observation methods and instrumentation, and are the basis for verifying and validating system performance. However, while instrumentation itself may meet specified requirements, their integration into an automatable system is challenging particularly for more complex systems such as NEON's eddy covariance (EC) measurements.

AMTD
8, 10983–11028, 2015

The EC technique is used worldwide across numerous ecosystems to directly measure the exchange of momentum, energy and atmospheric trace gases between the earth's surface and atmosphere (Aubinet et al., 2012; Baldocchi et al., 1988; Swinbank, 1951). A typical EC system consists of a fast-response 3-D sonic anemometer for wind measurements, and an infrared gas analyser (IRGA) for H_2O and CO_2 measurements, often with fundamental response times of ≤ 0.1 s. However, additional infrastructure such as the IRGA gas sampling system (GSS) can decrease frequency response. As a result, high-frequency spectral corrections can exceed several 10 %, in particular for water vapour (e.g., Ammann et al., 2006; Fratini et al., 2012; Ibrom et al., 2007). Active testing and research on optimizing GSS subsystems and system components have been underway at NEON (see Metzger et al., 2014) and ICOS (see De Ligne et al., 2014). These studies indicate that substantial improvements to the IRGA system frequency response could be made by re-examining its GSS and components therein. The objective of this study is thus to produce an optimal combination of IRGA and GSS that (i) maximizes system practicability, and (ii) minimizes high-frequency spectral losses. In this endeavour, quantitative NEON requirements were used to evaluate the feasibility and degree to which these objectives were achieved. The overarching goal for such system is to permit unbiased, operational deployment and data processing across more comprehensive time and space domains for addressing the "Grand Challenges of Environmental Science".

NEON selected an enclosed IRGA (LI-7200; LI-COR Biosciences, Lincoln, NE, USA) due to (i) instantaneous temperature and pressure compensation (Burba et al., 2012; Webb et al., 1980), (ii) improved frequency response compared to closed-path IRGAs (e.g., Burba et al., 2010; Fratini et al., 2012; Ibrom et al., 2007), and (iii) improved data coverage and lower maintenance compared to open-path IRGAs. We tested combinations of the LI-7200 and GSS components (intake tube, particulate filter, rain cap), both in the laboratory and in the field. Focused laboratory tests were performed to determine the general suitability of individual GSS components and their combinations. These tests addressed water ingress, pressure drop, as well as high-frequency spectral loss.

AMTD
8, 10983–11028, 2015

Subsequently, comprehensive field tests were performed at the Niwot Ridge US-NR1 AmeriFlux site (see http://ameriflux.ornl.gov/fullsiteinfo.php?sid=34) in July 2013 and July 2014. These tests covered a wide range of weather conditions including condensing humidity, and addressed the settings for intake tube and particulate filter heating, as well as IRGA GSS integral performance.

In Sect. 2 we introduce the laboratory and field tests, each accompanied by a description of the test objective, i.e. the NEON requirement to be evaluated. In Sect. 3 we present the test results, and discuss whether a specified requirement can be achieved. Lastly, in Sect. 4, we summarize our findings, and conclude whether and how the presented approach was useful for developing an integrated IRGA GSS.

2 Materials and methods

In the following, a set of laboratory tests are described for determining a suitable combination of GSS components (Sect. 2.1). Subsequently, field tests for determining the optimal heater setting and resulting frequency response are described (Sect. 2.2). Each test is accompanied by a description of the NEON requirement under evaluation. A complete list of NEON requirements regarding IRGA and GSS dimensioning is provided externally in our supplement (see https://w3id.org/smetzger/Metzger-et-al_2015_IRGA-GSS). Additional details can be found in the Data Availability section.

2.1 Laboratory tests

During system development at LI-COR and subsequent system optimization and testing at NEON and LI-COR, over 110 laboratory tests were conducted on the specific components external to the LI-7200 analyser, including intake tubes, filters, meshes, membranes, rain caps, insect screens, heating arrangements, etc. Also, various combinations of these components were tested over a 6-year period, from 2008 to 2014. The tests had a wide range of goals and criteria, ranging from water ingress into a verti-

AMTD
8, 10983–11028, 2015
Optimization of a gas sampling system for measuring eddy-covariance fluxes
S. Metzger et al.

cal tube to the frequency attenuation by a membrane, and were conducted by different laboratories using varying equipment. Due to limited space in this study, only the key procedures are described below in a generalized form to provide the overall schemes and algorithms of testing. The results were aggregated to provide the range of performance across multiple tests.

2.1.1 Rain cap water ingress

In order to maximize data coverage and to minimize uncertainties in the latent heat flux determination, the GSS should be designed to minimize water ingress (NEON requirement NEON.TIS.4.1615). Different rain cap designs were tested for water ingress in a series of laboratory tests. Figure 1 shows three final rain cap designs; LI-COR's old rain cap (LO) until 2013, part number 9972-054, LI-COR's new rain cap (LN) from 2014, part number 9972-072, and the new NEON rain cap design (NN). Tests were conducted at a mass flow rate (standard temperature (T = 20 °C) and pressure (p = 101.325 kPa) conditions) of 23 SL min^{-1} (standard litres per minute) to emulate the worst case scenario. This significantly exceeded the minimal recommended volumetric flow rate (at temperature and pressure of measurement location) of 10.5 L min^{-1} (litres per minute) and nominal recommended volumetric flow rate of 15 L min^{-1}. The rain caps were sprayed from the top and side with a water hose at rates of 12.1–16.3 L min^{-1}, including horizontal spray. Additional tests were conducted at 15 SL min^{-1} flow rate to establish whether a downward-oriented tube with 6.4 mm inner diameter (ID) would transport water upwards. Water ingress was observed, and the test concluded that a rain cap would indeed be required for the system to prevent or minimize water ingress. The latter corroborated the results reported for a downward-oriented tube without a rain cap from field tests conducted by ICOS (De Ligne et al., 2014).

AMTD
8, 10983–11028, 2015

2.1.2 Pressure drop

To avoid inaccuracies in IRGA performance caused by accumulating dirt (Fratini et al., 2014), a particulate filter with $\leq 2.0\,\mu m$ pore size should be positioned immediately downstream of the rain cap (NEON requirements NEON.TIS.4.2007, NEON.TIS.4.1628). However, particulate filters can induce substantial pressure drops. Consequently, attention needs to be paid to not exceed the manufacturer's recommended range of the differential pressure sensor in the IRGA sampling cell (10 kPa, NEON requirement NEON.TIS.4.1618). For this purpose, pressure drops were tested for 15 different filters and for the range of flow rates from 2 to 20 $SL\,min^{-1}$. The overall scheme for these tests included a mass flow controller regulating the flow rate, and pressure measurements upstream and downstream of the filter to measure the drop. One set of tests used Sierra Mass Flow Controller (C100M-DD-3-OV1, Sierra Instruments, Monterey, CA, USA) and Dwyer manometer (Series 477, Dwyer Instruments, Michigan City, IN, USA) in conjunction with compressed air from a cylinder to push air through the filter. Another set of tests used a LI-7200 Flow Module (Model 7200-101, LI-COR Biosciences, Lincoln, NE, USA) as a flow provider and flow controller to pull the air through the filter, and LI-7200 differential pressure measurements to record pressure drop. Yet other tests used a vacuum pump (1023-101Q-SG608X, Gast, Benton Harbor, MI, USA) in combination with a ballast chamber (5344R, Scott Specialty Gases, Plumsteadville, PA, USA) and barometer measurements upstream and downstream of the filter (PTB 330, Vaisala, Helsinki, Finland).

This study reports results for the 9 filters listed in Table 1. The ultimately selected FW-2.0 filter (Swagelok, Solon, OH, USA) was tested in several additional experiments and results are presented as a range of values from all the experiments.

2.1.3 High-frequency attenuation

In general, the transfer function $F_T(f)$ of a system is defined as the ratio of its output to its input as a function of the natural frequency f. In an ideal system the transfer function

AMTD
8, 10983–11028, 2015

would be unity across all frequencies. In a real system, fluctuations in CO_2 or H_2O tend to be dampened at higher frequencies. Using power spectra to quantify transfer functions, the output variance or covariance is reduced to 50 % or −3 dB of its input at the half-power frequency $f_{50\,\%}$. Adding a rain cap, filter and intake tubing to an IRGA essentially acts as a low-pass filter. That is, it attenuates high-frequency fluctuations of H_2O and CO_2, which subsequently reduces the turbulent flux calculated via correlation with the vertical wind speed measurement. In order to allow automated procedures for high-frequency spectral corrections (e.g., Nordbo and Katul, 2012), the combined frequency response of the IRGA and its GSS shall be un-attenuated at frequencies ≤ 1 Hz (NEON requirement NEON.TIS.4.1626). Moreover, early results showed a wide range of frequency response for the particulate filters. Based on the above objective and Eqs. (7)–(10) below, we additionally specified that the filter shall have a half-power frequency $f_{50\,\%} \geq 4$ Hz (NEON requirement NEON.TIS.4.1627).

The transfer function of an IRGA system including the GSS can never be better than the spectral quality of the IRGA itself. Consequently, first the frequency response of the IRGA needs to be quantified. This allows subsequent determination of whether and for which GSS components optimization can warrant significant frequency response improvements. The LI-7200 optical unit measures CO_2 and H_2O number density at internal rates exceeding 100 Hz. In combination with minimal inertia thermocouples and pressure transducers for mole fraction conversion, LI-7200 frequency response is likely dominated by volume averaging in the optical cell with a volume of $V = 16.0\,\text{cm}^3$. The volume averaging effect can be quantified by the generalized transfer function of Silverman (1968), in the form of Massman (2004) and Moore (1986):

$$F_\mathrm{T}(f) = \frac{\sin^2(\pi f \tau)}{(\pi f \tau)^2} \quad \text{with the time constant } \tau, \tag{1}$$

$$\tau = \frac{V}{Q_\mathrm{v}}, \tag{2}$$

AMTD
8, 10983–11028, 2015

Optimization of a gas sampling system for measuring eddy-covariance fluxes

S. Metzger et al.

π being number pi, and Q_v being volumetric flow rate. Analogously, Eq. (1) can be used to approximate the along-path (worst case) averaging effect of open-path gas analysers aligned to within $\approx 30°$ of horizontal by determining τ as:

$$\tau = \frac{d_l}{U}, \tag{3}$$

with length of the optical path d_l (e.g., 12.5 cm for a LI-COR LI-7500) and horizontal wind speed U.

Subsequently, high-frequency attenuation was tested for the IRGA and each separate component of the GSS, as well as for cross-combinations of components, and for the complete system consisting of all listed components (Table 2). Two techniques were used for this purpose: (i) providing a CO_2 and H_2O change as a singular rising or falling step, and (ii) generating a square wave consisting of a sequence of many rising or falling steps. While (i) allows efficiently pre-screening a large number of parts, only (ii) provides the necessary sample size for determining stable results based on Fourier Transformation. The Fourier Transform of a perfect square waves' time derivative would show similar contributions across all frequencies, and the Fourier Transform of the actual time series' time derivative is the systems transfer function (Truax, 1999). In all experiments, solenoid switches were used to rapidly alternate between zero air and pre-defined concentrations of CO_2 and H_2O upstream of the tested component. The corresponding change was measured with a LI-7200 downstream of the tested component. In H_2O and CO_2 experiments the relative humidity (RH) and dry mole fraction varied between 0–90 % and 0–400 ppm, respectively. For H_2O specifically, the moist airstream was maintained at RH > 90 % to reflect the field environment as well as possible. Nevertheless, for the square wave, the time-average over alternating dry and moist airstreams cannot exceed RH = 50 %. A dew point generator (for lower flow rates: LI-610, LI-COR Biosciences, Lincoln, NE, USA) or bubbler (for higher flow rates) in combination with a hygrometer (Optisure, Kahn Instruments, Wethersfield, CT, USA) were used to generate, control and record H_2O concentrations. Tests were performed for a minimum of 420 s, and LI-7200 variables were recorded at 50 Hz. In these tests,

AMTD
8, 10983–11028, 2015

flow rates ranged from 9 to 35 SLPM depending on the experiment's goal, providing fully turbulent tube flow in the vast majority of tests (Reynolds number, Re > 4000) or upper range of transient flow in a few tests (Re > 3300).

Prior to the power spectra analysis (i) the first 200 s and last 20 s of data were discarded to focus on steady-state periods, (ii) missing values were linearly interpolated, (iii) the dry mole fraction time-derivative was calculated, (iv) the time-derivative was low-pass filtered with a 5th order Butterworth filter at 15 Hz half-power frequency to dampen leaking from high frequencies, (v) linear de-trending was applied to minimize bias, and (vi) 5 % of the data at each end of the time series are tapered with a cosine-bell to reduce bias and to avoid leaking of peaks at far-away frequencies into other parts of the spectrum. Next, a fast Fourier transform was applied and unfolded spectral energy and co-spectra were calculated. A recursive circular filter with a Daniell kernel was then used to reduce noise, and the resulting Fourier coefficients were binned into exponentially widening frequency classes using the arithmetic mean. The result for the LI-7200 without additional GSS components $S_{\mathrm{ref}}(f)$ corresponds to the reference transfer function of the LI-7200 in combination only with the experimental setup (solenoids, connectors, etc.). The results for the LI-7200 with additional GSS components $S_{\mathrm{test}}(f)$ correspond to the test transfer functions of the LI-7200 in combination with the experimental setup as well as filter, intake tube and rain cap. Transfer functions $F_{\mathrm{T}}(f)$ of filter, tube, rain cap as well as their combinations independent of LI-7200 and experimental setup were calculated by division of the individual power spectra (e.g., Foken et al., 2012). For this it is assumed that the mean spectral response between $f_1 = 0.01$ Hz and $f_2 = 0.2$ Hz was not attenuated:

$$F_{\mathrm{T}}(f) = R_{\mathrm{N}} \frac{S_{\mathrm{test}}(f)}{S_{\mathrm{ref}}(f)}, \quad \text{with the dimensionless normalization factor;} \tag{4}$$

$$R_{\mathrm{N}} = \frac{\int_{f_1}^{f_2} S_{\mathrm{test}}(f)\mathrm{d}f}{\int_{f_1}^{f_2} S_{\mathrm{ref}}(f)\mathrm{d}f}. \tag{5}$$

AMTD
8, 10983–11028, 2015

Noise was reduced by a circular filtering with a Daniell kernel. In cases where multiple test results were available, ensemble transfer functions and their ranges were calculated. Finally, $f_{50\,\%}$ was determined by inter/extrapolation of the resulting transfer function coefficients using the sigmoidal model of Eugster and Senn (1995):

$$F_{\mathrm{T}}(f) = \frac{1}{1 + \left(\frac{f}{f_{50\,\%}}\right)^2}. \tag{6}$$

Resistor-capacitor theory then allows determining $f_{50\,\%}$ for a resulting system when multiple passive low-pass filters are combined, such as rain cap, filter and tube (e.g., Williams and Taylor, 2006):

$$f_{50\,\%} = 1.54\, f'_{50\,\%} - 4.66\,\mathrm{Hz}, \quad \text{with the non-damped half-power frequency;} \tag{7}$$

$$f'_{50\,\%} = f_{\mathrm{h}} \sqrt{2^{\frac{1}{n}} - 1}, \quad \text{the harmonic frequency;} \tag{8}$$

$$f_{\mathrm{h}} = \frac{1}{2\pi \sqrt[n]{\prod_{1}^{n} \tau_n}}, \quad \text{and the time constant } \tau_n \text{ for each low-pass filter } n; \tag{9}$$

$$\tau_n = \frac{1}{2\pi f_{50\,\%,n}}. \tag{10}$$

The systems' damping coefficients in Eq. (7) were determined from an unweighted least-squares regression ($R^2 = 0.92$, p value $= 6.338 \times 10^{-8}$): measured $f_{50\,\%}$ for several combinations of rain cap, filter and tube ($N = 14$) were regressed against $f'_{50\%}$ calculated from measured $f_{50\%}$ for individual components using Eqs. (8)–(10).

In addition to physical laboratory tests, high-frequency attenuation processes were also modelled using computational fluid dynamics (CFD) software (ANSYS, Canonsburg, PA, USA). To corroborate the experimental results, turbulent flow simulations of cases with well-mixed and plug-flow assumptions were performed. The CFD results

AMTD
8, 10983–11028, 2015

consistently showed lower attenuation by the components than experimental data, indicating that a perfect step change or a perfect square wave is not achievable in real-life settings.

A variety of additional aspects need to be considered and warrant testing when optimizing an IRGA GSS. Of these, heating of the tube, filter and other components are addressed by the field experiments in this study (Sects. 2.2, 3.2), and by Fratini et al. (2012). Other tests are not the focus of this paper, such as optimization of tube length, tube material and flow rates, which have been covered both conceptually and experimentally by Burba et al. (2010); Clement et al. (2009); Fratini et al. (2012); Massman and Ibrom (2008); Rannik et al. (1997); Runkle et al. (2012).

2.2 Field tests

In July of 2013 and 2014 field tests were performed at the Niwot Ridge Subalpine Forest AmeriFlux US-NR1 site (see http://ameriflux.ornl.gov/fullsiteinfo.php?sid=34). The objectives of these tests were to determine (i) the impact and suitable dimensioning of intake tube heating, and (ii) whether the final GSS provides sufficient high-frequency response to warrant automated high-frequency spectral corrections in post-processing. To prevent condensation and to minimize attenuation of the water vapour measurement, the IRGA intake tube should be insulated and continuously heated with a constant wattage (NEON requirement NEON.TIS.4.2017). However, to enable mole fraction conversions to within manufacturer performance specifications, the temperature difference between IRGA inlet and outlet should be maintained to within $\leq 5\,^{\circ}$C (NEON requirement NEON.TIS.4.1668). To ensure that IRGA drift with temperature remains within manufacturer performance specifications, the temperature difference between the IRGA block and inlet should be maintained to within $\leq 15\,^{\circ}$C (NEON requirement NEON.TIS.4.1667). Lastly, to sufficiently improve H_2O frequency response for automated high-frequency spectral corrections, the heating wattage should be chosen so that relative humidity in the IRGA is maintained at $\leq 60\,\%$ (NEON requirement

NEON.TIS.4.1666). Below this threshold, H_2O high-frequency attenuation behaves principally similar to CO_2 (e.g., Fratini et al., 2012).

2.2.1 Site description

US-NR1 is located in the Rocky Mountains, Colorado, USA (40°1′58″ N, 105°32′47″ W, 3050 m elevation), where measurements began in November 1998 (Monson et al., 2002; Turnipseed et al., 2002, 2003). The forest near the tower is around 110 years old, and primarily composed of subalpine fir (*Abies lasiocarpa var. bifolia*), lodgepole pine (*Pinus contorta*), and Englemann spruce (*Picea engelmannii*). The tree density is around 0.4 trees m^{-2} with a leaf area index of 3.8–4.2 $m^2\ m^{-2}$, tree heights of 12–13 m (Monson et al., 2010; Turnipseed et al., 2002) and an approximate displacement height of 7.8 m.

2.2.2 Instrumentation

All instrumentation used in the field tests was deployed on the US-NR1 tower at 21.5 m above ground, equivalent to 13.7 m above the displacement height. The companion study by Burns et al. (2014) provides an in-depth description of the sensor deployments, in short:

A Vaisala HMP35-D platinum resistance thermometer and capacitive hygrometer (Vaisala, Helsinki, Finland) was sampled at 1 Hz and was used in this study as reference for ambient air temperature (T_a) and relative humidity (RH_a).

A CSAT3 sonic anemometer (Campbell Scientific, Logan, UT, USA, S/N 0254, firmware v4) was used to measure the turbulent wind components. The measurements were performed in single-measurement mode at 10 Hz sampling rate, collected using the Campbell Scientific SDM protocol, and synchronized with variables from other sensors using network timing protocol (NTP). From the CSAT3, the along-axis, cross-axis and vertical-axis wind components as well as sensor health information (from the CSAT3 diagnostic word) were used in this study.

AMTD
8, 10983–11028, 2015

Infrared gas analysers were used to measure the turbulent fluctuations of H_2O and CO_2. A LI-7500 open-path IRGA (LI-COR Biosciences, Lincoln, NE, USA, S/N 75H-0084, firmware v2.0.4) was used as a reference for high-frequency response. The LI-7500 optical path was vertically centred with the CSAT3 sonic path, and laterally separated by 30 cm until 8 October 2013 and ≈ 90 cm thereafter. Data were collected at 10 Hz sample rate and 20 Hz bandwidth settings, and synchronized with variables from other sensors using NTP. From the LI-7500, H_2O and CO_2 number densities were used in this study. A LI-7200 enclosed IRGA (LI-COR Biosciences, Lincoln, NE, USA, S/N 72H-0192 until 2 November 2013, S/N 72H-0479 thereafter, both firmware v6.5.2) was used to study the impact of GSS intake tube heating and rain cap on high-frequency response. The LI-7200 rain cap was vertically centred with the CSAT3 sonic path, and laterally separated by 30 cm until 12 November 2013 and 22 cm thereafter. The measurements were performed with a flow rate setting of 10.8 $SL\,min^{-1}$. At the ambient air density this resulted in approximately 16.2 $L\,min^{-1}$ volumetric flow rate, or a ≈ 16 Hz renewal rate of the 16.0 cm^3 LI-7200 optical cell assuming plug-flow. Data were collected at a 20 Hz sample rate and 10 Hz bandwidth settings using the LI-7550 analyser interface, and synchronized with variables from other sensors using precision timing protocol. From the LI-7200, H_2O and CO_2 number densities, inlet, outlet and block temperatures of the optical cell (T_{in}, T_{out}, T_{block}, respectively), as well as sensor health information were used in this study.

During the field tests, the LI-7200 GSS consisting of a rain cap, connected to a FW-2.0 filter and a stainless steel tube were tested. Until 7 January 2014, the LO rain cap (Fig. 1) was used in combination with a 70 cm long 4.8 mm ID tube. Thereafter, a prototype of the LN rain cap was used in combination with an 80 cm long 5.3 mm ID tube. Both, tube and filter were uniformly covered by a Watlow 010300C1 100 Ohm heating element rated at 120 V and 150 W (Watlow Electric, St. Louis, MO, USA). A tight fit and thermal contact was ensured by plastic spiralling, followed by AP/Armaflex closed-cell elastomeric thermal insulation with 12.7 mm ID and 9.5 mm wall thickness (Armacell International, Capellen, Grand Duchy of Luxembourg) and white heat shrink. A Tenma

AMTD
8, 10983–11028, 2015

72–7705 power supply rated at 60 V and 6 A (Tenma Test Equipment, Washington, OH, USA) was used to test different heating power settings.

2.2.3 Data processing

An analysis package developed in GNU R version 3.1.3 (R Development Core Team, 2012) was used for data processing. This package is described in detail in Metzger et al. (2012, 2013), has been verified against other turbulence processors (e.g., Mauder and Foken, 2011) and is available upon request. Relevant processing steps are: all data were prepared by first regularizing to evenly-spaced time increments, which are exactly 1 s for HMP35, 0.1 s for CSAT3 and LI-7500, and 0.05 s for LI-7200, respectively. Next, observations with invalid sensor health information were discarded, thresholds for physically feasible value ranges were applied, and spikes were removed using the median filter method by Brock (1986). Thereafter, the wind components were rotated into the 14 month average aerodynamic plane using the planar fit rotation (Wilczak et al., 2001), and all slow-sample variables (1, 10 Hz) were linearly interpolated to 20 Hz with zero gap tolerance. Finally, lag times resulting from lateral separation and gas transport in the GSS were determined via cross-correlation in a 1 s window over high-pass filtered data (4-pole Butterworth filter with half-power frequency at 0.5 Hz) and shifted on a 30 min basis. Intake tube heating power was interpolated between site visits with $R^2 > 0.99$ and 0.38 K residual standard error using the difference between T_{in} and T_{out} as well as a unique identifier for each tube as predictors.

Prior to power spectra analysis on a 30 min basis, missing values were linearly interpolated. Linear de-trending was applied and 5 % of the data at each end of the time series were tapered with a cosine-bell. Next, a Fast Fourier transform was applied and unfolded spectral energy and co-spectra were calculated. Where indicated, a recursive circular filter with a Daniell kernel was used to reduce variance for graphical presentation. The resulting Fourier coefficients were binned into exponentially widening frequency classes using the median operator. Transfer functions were derived following Eqs. (4) and (5) by dividing the H_2O and CO_2 number density power spectra

Discussion Paper | Discussion Paper | Discussion Paper | Discussion Paper |

AMTD

8, 10983–11028, 2015

Optimization of a gas sampling system for measuring eddy-covariance fluxes

S. Metzger et al.

from the LI-7200 through those from the LI-7500, and normalizing to the same spectral power between 0.005 and 0.05 Hz. The determination of the half-power frequency was then automated in the following way: (i) determining the frequency > 0.5 Hz for which the transfer function reaches its first minimum, (ii) recasting the transfer function Eq. (6) and solving for half-power frequency. Lastly, the spectral correction factors for the corresponding EC fluxes were determined by applying the transfer functions to the co-spectra of H_2O and CO_2 dry mole fraction and the vertical wind speed.

Before calculating the ensemble power spectra, all available periods were screened for (i) recorded maintenance activities and interruptions, and > 90 % raw data coverage (78 % half-hours remained), (ii) successful lag correction (70 % half-hours remained), (iii) undisturbed inflow sector (65 % half-hours remained), and (iv) measured variations in H_2O and CO_2 number density in excess of 5 : 1 signal-to-noise (instrument resolution) ratio (Lenschow and Sun, 2007, 46 % half-hours remained).

Lastly, in order to attribute the effect of intake tubes with different length d_l and inner diameter d_{id}, we solved the transfer function proposed by Philip (1963) in the form of Massman (1991) for half-power frequency:

$$f_{50\,\%} = \frac{\sqrt{\frac{-\ln\left(\sqrt{0.5}\right)U^2}{\Lambda(Re)d_l\frac{d_{id}}{2}}}}{2\pi} \tag{11}$$

with the longitudinal mean flow velocity in the tube U, and a linear interpolation of tabulated values (Table 1 in Massman, 1991) for the attenuation coefficient Λ (Re) (Lee and Gill, 1977, 1980).

3 Results and discussion

In the following, results for individual GSS components and their combinations are presented, based on laboratory tests (Sect. 3.1). Subsequently, the effect of different

AMTD
8, 10983–11028, 2015

heater settings and resulting frequency response for combined IRGA and GSS systems are shown, based on additional field tests (Sect. 3.2).

In order to determine the significance of GSS optimization, first of all the LI-7200 frequency responses were calculated. Numerically evaluating Eqs. (1) and (2) for Q_v leads to the simple linear relationship $Q_v = f_{50\,\%} \times 2.167\,\mathrm{LPM\,Hz^{-1}}$ ($R^2 = 1$; p value $< 2.2 \times 10^{-16}$). The minimum required volumetric flow rate to achieve the most stringent half-power frequency requirement of $f_{50\,\%} > 4\,\mathrm{Hz}$ for the particulate filter can then be determined to be $> 8.7\,\mathrm{L\,min^{-1}}$. Thus, at larger flow rates, the LI-7200 itself does not limit the objectives of the GSS optimization. For the flow rate set point of $10.8\,\mathrm{SL\,min^{-1}}$ (corresponding to $\approx 13.6\,\mathrm{L\,min^{-1}}$ and $\approx 16.2\,\mathrm{L\,min^{-1}}$ under laboratory and site conditions, respectively), the LI-7200 operates at $f_{50\,\%} = 6.3\,\mathrm{Hz}$ and $f_{50\,\%} = 7.5\,\mathrm{Hz}$, respectively.

3.1 Laboratory tests

All high-frequency attenuation experiments suffered from the intrinsic inability to produce a perfect step change or a perfect square wave under real-life conditions. Response time of the laboratory setup (solenoids, effects of connectors and other physical mixing volumes upstream of a tested component) attenuate the step change itself. This resulted in an apparent reduction in frequency response of a tested component. A remedy was to normalize the results of the LI-7200 in combination with GSS components to the LI-7200 alone. Such procedure not only allowed the unveiling of the individual transfer functions of each GSS component, but also compensated for setup differences and enabled cross-comparison and aggregation of the results from the numerous different experiments. From our laboratory frequency response tests with the LI-7200 alone, we found $f_{50\,\%} = 3.4\,\mathrm{Hz}$ for the combined effects of the LI-7200 and the laboratory setup. Using this together with $f_{50\,\%} = 6.3\,\mathrm{Hz}$ for the LI-7200 itself in Eqs. (7)–(10) and solving numerically yields $f_{50\,\%} = 10.6\,\mathrm{Hz}$ for the laboratory setup.

AMTD
8, 10983–11028, 2015

3.1.1 Optimization of a rain cap

An important part of optimizing an enclosed IRGA EC system is determining which arrangement provides the best frequency response of the entire system. This would obviously be achieved by using a very short tube in the absence of any filter or rain cap. However, for the practical reason to prevent precipitation from entering the filter and sampling cell, most experimental sites would benefit from using a rain cap. The rain cap is a mixing volume in interaction with the atmosphere, and a focus of our optimization is to determine which rain cap design provides the least frequency attenuation, while still preventing water ingress into the tube, filter and sampling cell.

Numerous rain cap designs have been tested conceptually using the CFD software to minimize sample mixing in the rain cap. Several designs have been selected, built and tested to limit water ingress in the laboratory experiments, and rain caps that ingested liquid water when sprayed horizontally while operating at $23\,\mathrm{L\,min^{-1}}$ flow were rejected. In addition, we found that adding a slight downward tilt to the intake tube ($\approx 10^{\circ}$ from horizontal) helped avoid water ingress during the field tests (Sect. 3.2), which included periods of heavy precipitation. Consequently, the NEON requirement (NEON.TIS.4.1615) was fulfilled for the remaining designs, which were tested in the laboratory for frequency response following Eqs. (4) and (5). Figure 2 (top left panel) shows good frequency performance for LN and NN rain caps, with $f_{50\,\%} \geq 14.3\,\mathrm{Hz}$ and $f_{50\,\%} \geq 11.8\,\mathrm{Hz}$, respectively (Table 3 provides an overview for all system components). Both newer rain caps considerably exceeded the performance of the older LO rain cap ($f_{50\,\%} \geq 2.4\,\mathrm{Hz}$). However, both designs were still more limiting to high-frequency response compared to the filters with the best frequency response tested in Sect. 3.1.2.

ICOS conducted field tests of several additional rain caps for their LI-7200-based flux systems (De Ligne et al., 2014): (i) LI-COR's rain cap before 2013, part number 9972-043, which is a previous version of the LO rain cap, (ii) a modification of this rain cap with tubing extending all the way to the screen, (iii) a custom-built rain cap with lateral insertion and small volume were tested alongside (iv) a downward-oriented tube

AMTD
8, 10983–11028, 2015

without a rain cap and (v) the LN rain cap. The range of results ($1.4 \le f_{50\,\%} \le 7.9$ Hz) was similar to our tests but slightly lower. Differences may be attributed to differing gas injection design in the laboratory, different experiment settings required for the field testing, and possible filter contamination. Their conclusion was that the frequency response of the LN rain cap assembly (6.4 ± 1.0 Hz) was second only to the downward-oriented tube, and the latter was found to provide insufficient water ingress protection. The experiments of De Ligne et al. (2014) also concluded that the rain cap critically contributes to overall system frequency response.

3.1.2 Optimization of a particulate filter

Similar to the rain cap situation, the highest frequency response of an enclosed IRGA EC system would be achieved without using a particulate filter. Such configurations are possible for a system based on the LI-7200 analyser, and have previously been used in the field (Burba et al., 2010, 2012; Clement et al., 2009). However, they would require frequent cleaning of the sampling cell in dusty environments or during high-contamination periods (e.g., harvest, pollination, etc.). To reduce the demand for cleaning, an intake particulate filter can be used. The important trade-off when optimizing the filter is to determine which models provide the least frequency attenuation with the smallest pressure drop, and still provide a pore size small enough to filter out most of the ambient particular contaminants. Figure 3 shows results from multiple laboratory experiments for such an optimization. Out of nine tested filters, the Swagelok FW-2.0 filter (Table 1 provides detailed filter specifications) had the lowest pressure drop (0.2 kPa at 10 SL min^{-1}), reasonably small high-frequency attenuation ($f_{50\,\%} \ge 14.9$ Hz), and still provided 2.0 µm particular filtering. The ZenPure PF-0.1 filter was a close second in pressure drop (0.6 kPa at 10 SL min^{-1}), but its frequency attenuation for CO_2 was much worse than the FW-2.0 at the high frequency range ($f_{50\,\%} \ge 8.3$ Hz), and its attenuation for H_2O was unacceptable ($f_{50\,\%} \ge 1.4$ Hz). Other tested filters had much larger pressure drops, which are not desirable for high-quality dry mole fraction computation, and which unnecessarily increase power consumption and wear on the system.

AMTD
8, 10983–11028, 2015

ICOS conducted field tests of several additional filters for their LI-7200-based flux systems (De Ligne et al., 2014). A Pall open-face 2 µm filter (Pall Corporation, Port Washington, NY, USA) was tested for pressure drop alongside the FW-2.0 and AC-1.0. The AC-1.0 pressure drop was found unacceptable, and Pall 2 µm open-face filter was found to be less effective in contamination prevention as compared to the FW-2.0 filter. The pressure drop for the FW-2.0 filter in the De Ligne et al. (2014) experiments was small, on the order of 0.9 kPa for 10 L min^{-1} at approximately sea level, but still 4–5 times the pressure drop found in our study. De Ligne et al. (2014) do not present half-power frequencies for individual GSS components, but state that addition of one of those filters did not significantly reduce LI-7200 system frequency response. The overall conclusion from both studies was similar suggesting the FW-2.0 filter to be optimal out of all tested models, and fulfilling the relevant NEON requirements (NEON.TIS.4.2007, NEON.TIS.4.1628, NEON.TIS.4.1618, NEON.TIS.4.1627).

3.1.3 Interaction of system components

Depending on the interaction of the system components reflected by Eq. (7), the total frequency response of the system may differ from a superposition of all components according to Eqs. (8)–(10). Hence, experiments were conducted to determine the actual effect of combining various system components on the total frequency response of the system, i.e. to parameterize Eq. (7). Figure 2 (top right and bottom panels) shows the results of such experiments for three main practical combinations of the components: (i) tube and filter, (ii) tube and rain cap, and (iii) combination of tube, filter and rain cap deployed together. Table 3 summarizes these and other results of laboratory experiments for various filters, rain caps, and their combinations.

Combining the tube and the FW-2.0 filter leads to a very minor effect on CO_2 frequency response as expected from the small volume of the filter and turbulent tube flow (11.9 Hz $\leq f_{50\,\%} \leq$ 15.4 Hz, Fig. 2 top right panel and Table 3). The H_2O response was noticeably affected, although to a relatively small degree (11.2 Hz $\leq f_{50\,\%} \leq$ 11.6 Hz). Such reduction in H_2O frequency response is expected because both filter and espe-

AMTD
8, 10983–11028, 2015

cially the tube have large surface areas in relation to the sample volume and flow. The dipolar nature of the water molecule and surface adsorption/desorption rates proportional to relative humidity lead to a "sticky" behaviour of water vapour at the tube and filter surfaces. Such phenomenon was studied, modelled, and corrected for in a number of studies (e.g., Fratini et al., 2012; Massman and Ibrom, 2008; Rannik et al., 1997; Runkle et al., 2012). It can be partially remedied by heating the elements to reduce the relative humidity at the wall surface below 50–60 %. Below this threshold, H_2O behaves principally similar to CO_2 and theoretical corrections can be used to compensate for the frequency losses (Kaimal et al., 1972; Moncrieff et al., 1997). In the absence of heating, semi-empirical corrections progressive with relative humidity can also be used (e.g., Fratini et al., 2012; Massman and Ibrom, 2008; Runkle et al., 2012).

Combining the tube and rain cap led to a larger reduction in frequency response than combining the tube and filter for both CO_2 and H_2O (2.0 Hz $\leq f_{50\,\%} \leq$ 12.0 Hz, Fig. 2 bottom left panel and Table 3). In fact, out of all elements in the system, the rain cap appeared to have the largest effect on the GSS frequency response. The importance of the rain cap choice was somewhat a surprise given that traditional closed-path GSSs utilize various custom-made rain caps with volumes exceeding several times those shown in Fig. 1. Yet, recent analyses by NEON (Metzger et al., 2014) and ICOS (De Ligne et al., 2014) corroborated the importance of the rain cap size and construction as a very sensitive component affecting EC system frequency response. The CFD simulations (data not shown) suggested that even small rain caps may experience vortices such that residence time of the sample in the rain cap exceeds that computed by simply dividing a rain cap volume by a flow rate (plug flow). This may explain why rain caps are responsible for a significant reduction in system frequency response in comparison to other components such as a short tube and a filter.

The frequency response of the combination of all elements in an enclosed IRGA EC system is shown in Fig. 2 (bottom right panel). The worst response was observed for the combination of the tube, FW-2.0 filter and the LO rain cap. This response was primarily driven by the effects of the rain cap (Fig. 2, top left panel) and yielded

AMTD
8, 10983–11028, 2015

$f_{50\,\%} \geq 2.0$ Hz for the entire GSS for both CO_2 and H_2O (Table 3). Using the new, smaller rain caps significantly improved GSS system response, with half-power frequencies 2–6 times higher than with the LO rain cap. Differences among the GSS with the NN ($f_{50\,\%} \geq 9.3$ Hz) and LN ($f_{50\,\%} \geq 4.3$ Hz) rain caps were noticeable for both, CO_2 and H_2O, but overall both rain caps were much closer to each other compared to the LO rain cap. Also, these differences may be biased due to different sampling techniques, levels of relative humidity, and by how a step change or a square wave were generated in the laboratories. These tolerances were also apparent from a slightly better frequency response for the combination of tube, FW-2.0 filter and NL rain cap ($f_{50\,\%} = 12.0$ Hz) compared to the setup omitting the FW-2.0 filter ($f_{50\,\%} = 11.9$ Hz). Moreover, the laboratory tests of the NN rain cap did not include any dead volume potentially created by the rain caps' outer lip and leaking into the sample flow. While this lip adds rain protection and is vertically offset, it might increase air residence time in the vicinity of the rain cap, thus potentially providing a better response in the laboratory than might be attainable under field conditions.

Overall, we found that possible choices of filters ($f_{50\,\%} \geq 1.4$ Hz) and rain caps ($f_{50\,\%} \geq 1.9$ Hz) limit system frequency response compared to the LI-7200 sampling cell ($f_{50\,\%} \geq 6.3$ Hz) and a short and thin intake tube ($f_{50\,\%} \geq 15.9$ Hz). In order to better understand cross-sensitivity, we utilized Eqs. (7)–(10) and determined the frequency responses for all possible combinations of filters and rain caps, including those not explicitly tested (Fig. 4). It can be seen that for H_2O, the NN and LN rain caps provided similar frequency response, up to $\Delta f_{50\,\%} = 5$ Hz better compared to the LO rain cap. Yet, for NN and LN rain caps, the filter choice can decrease frequency response by as much as $\Delta f_{50\,\%} = -6$ Hz. For the LO rain cap, the effect of the filter choice was less pronounced, with a decrease in frequency response by as much as $\Delta f_{50\,\%} = -2$ Hz. It should be noted that for the two slowest filters AC-1.0 and PF-0.1, we determined $f_{50\,\%} < 0$, which is not physically feasible. However, the magnitude of underestimation falls within the standard error of regression Eq. (7). For CO_2, the difference between NN and LN rain caps was slightly more pronounced compared to H_2O, with the NN rain cap

AMTD
8, 10983–11028, 2015

providing $\Delta f_{50\,\%}$ ≈1 Hz better frequency response. Regardless, both rain caps provided frequency responses as much as $\Delta f_{50\,\%}$ = 6 Hz better when compared to the LO rain cap. The filter choice can decrease frequency response by as much as $\Delta f_{50\,\%}$ = −4 Hz and $\Delta f_{50\,\%}$ = −2 Hz for the NN and LN rain caps, and the LO rain cap, respectively. Our results also indicate that in terms of frequency response, the least favourable combinations studied here were the LO rain cap and AC-1.0 or PF-0.1 filters.

To summarize, from laboratory tests, the order of priority for optimizing GSS components against frequency response should be the choice of (i) rain cap, (ii) particulate filter, and (iii) intake tube. The NN and LN rain caps in combination with the FW-2.0 filter provided the best and most comparable frequency response for both, H_2O and CO_2 ($f_{50\,\%} \geq 7$ Hz). To also permit switched heating during icing conditions, NEON developed the NN rain cap. However, the NN rain cap was not yet available at the time of the experiments, so the remaining analysis will focus on the LN rain cap.

3.2 Field tests

All laboratory tests were conducted without heating or insulation. However, both NEON and LI-COR were working towards integrated heating designs to maximise the system frequency response, which is addressed in this section. Field tests focused on the effect of heating on GSS consisting of the LO and LN rain caps in combination with the FW-2.0 filter and an intake tube. Here, we selected two periods (i) July 2013 to compare the effect of different heater settings on frequency response with the LO rain cap, and (ii) July 2014 to compare the effect of LN vs. LO rain cap on frequency response at a given heater setting.

3.2.1 Experiment and sensor conditions

Figure 5 shows the meteorological conditions and the effect of filter and intake tube heater settings for July 2013 with the LO rain cap. It can be seen that the LI-7200 sampling cell inlet temperature increased above the ambient air temperature due to

AMTD
8, 10983–11028, 2015

heating, and generally followed the heater power setting. The initial 4 W of heating power increased the sampling cell inlet temperature by about 6–8 °C above ambient, and after the heating was switched off on 7 July 2013, this difference decreased to 0–3 °C above ambient. During both settings, the temperature gradient in the sampling cell did not exceed 5 °C, and the temperature difference between the sampling cell inlet and block was well below 15 °C. However, during the 5 and 6 W settings, the temperature gradient in the sampling cell exceeded 5 °C. Consequently, the relevant NEON requirements (NEON.TIS.4.2017, NEON.TIS.4.1668, NEON.TIS.4.1667) were only fulfilled for the 4 W heater setting. At a given power setting, the increase in sampling cell inlet temperature above ambient was correlated with the ambient temperature. For example, during the 4 W heating period, per 1 °C rise in ambient temperature, the sampling cell inlet temperature increases by 1.26 °C ($r > 0.7$). Similar behaviour was found without heating (1.29 °C per 1 °C, $r > 0.7$). Consequently, the heating circuit does not exhibit a feedback with ambient temperature, thus avoiding the risk of superimposing artificial correlations. After water ingress on 14 July 2013, the intake tube was changed from horizontal to downward tilted (≈ 10°) alignment, which avoided any future ingress. The new tube was deployed with identical heating power setting. Yet, it is apparent that the replacement tube generated more heat than the previous tube, indicating an impact of variable manufacturing tolerances.

In order to avoid sensor offsets, relative humidity in the LI-7200 cell (RH_{cell}) was calculated from the ambient relative humidity (RH_a) taking into account temperature and pressure differences. Compared to RH_a, RH_{cell} was reduced by ≈ 10, ≈ 20, ≈ 25 and ≈ 30 % during the 0, 4, 5 and 6 W heating periods, respectively. However, none of the tested heater settings was capable of continuously reducing RH_{cell} below 60 %, and therefore the corresponding NEON requirement (NEON.TIS.4.1666) could not be fulfilled at this time. Nevertheless, 4 W of heating was sufficient to decrease the number of events where $RH_a > 60$ % resulted in $RH_{cell} > 60$ % by ≈ 50 %.

Table 4 provides descriptive statistics of temperatures and humidities for all heating periods utilized in this study. In addition to the periods shown in Fig. 5, Table 4 also

AMTD

8, 10983–11028, 2015

includes the period in July 2014 where the LN rain cap was deployed. The median ambient temperature and relative humidity varied in a range of 3.3 ± 5.6 °C and 22.6 ± 28.6 % among heating periods, respectively. Specifically, the LO-0 Watt period was driest with RH_a = 46.1 %, making it difficult to find periods of high relative humidity for intercomparison. The LO-6 Watt period was the most humid with RH_a = 68.7 %.

3.2.2 Spectral analysis

Spectral analysis as described in Sect. 2.2.3 was performed on the field data, and Fig. 6 shows ensemble transfer functions of LI-7200-measured H_2O number density relative to the LI-7500. In all cases, heating improved the high-frequency response. For $RH_a < 60$ %, the half-power frequency of the LO rain cap in combination with unheated filter and intake tube was $f_{50\,\%} \approx 2$ Hz. This confirms the laboratory results for the LO rain cap in combination with filter and tube. Filter and intake tube heating marginally increased $f_{50\,\%}$ to ≈ 2.5 Hz. For $RH_a > 60$ %, $f_{50\,\%}$ of the LO rain cap in combination with the unheated filter and intake tube decreased to ≈ 1 Hz. This is about half of the $f_{50\,\%}$ observed in the laboratory, but the latter could not actually be conducted at such high average relative humidity. Also, it should be noted that the sample size of the LO-0 Watt control period was extremely small for $RH_a > 60$ % (here, $N = 3$, due to the generally low relative humidity in this period, median 46.1 %). Filter and intake tube heating increased $f_{50\,\%}$ to ≈ 1.5–2 Hz, and the 4 and 5 W heating power settings yielded a slightly higher $f_{50\,\%}$ compared to the 6 W setting, which was likely a result of the higher ambient relative humidity during the LO-6 Watt period.

The LI-7500 was configured with 10 Hz sample rate and 20 Hz bandwidth. This makes aliasing possible, which, however, was not observed. Instead, at $RH_a > 60$ % and with 5 W heating the transfer function for the LO rain cap indicated that the LI-7200 setup produced noise above ≈ 2 Hz: in comparison to the LI-7200 cell, frequency response due to line-averaging over the 12.5 cm long LI-7500 optical path was variable, with $f_{50\,\%} > 7.5$ Hz for wind speeds exceeding 1.4 m s^{-1} (i.e., better than the frequency response of the LI-7200 cell at ≈ 16.2 L min^{-1}). Moreover, the LI-7500 measured the

AMTD
8, 10983–11028, 2015

full effect of temperature fluctuations on density. So some of the fluctuations in density were large and well-resolved, but they did not actually contribute to the turbulent flux. In contrast, temperature-related density fluctuations are mostly attenuated in the LI-7200 cell (Burba et al., 2012).

Overall, no obvious improvement of H_2O frequency response was found for increasing heating power beyond 4 W. The resulting 8 °C temperature increase above ambient appeared to be sufficient, and the remaining field tests will focus on this heater setting, which is the only setting that also fulfils NEON's corresponding requirements (NEON.TIS.4.2017, NEON.TIS.4.1668, NEON.TIS.4.1667). Since the rain cap has been identified as a design priority in Sect. 3.1, we expected that decreasing the rain cap mixing volume would further improve frequency response for H_2O. However, for the 4 W heating setting, the LN rain cap did not appear to outperform the LO rain cap. This contradicts our laboratory findings, which suggest $f_{50\,\%} > 4$ Hz for the combination of LN rain cap with filter and tube. Also, during the LN rain cap period, filter and tube heating was actually 0.3 ± 0.9 W higher and RH_a was -13.1 ± 35.5 % lower compared to the corresponding LO rain cap period, which should have given the LN rain cap a slight advantage.

For the LN rain cap, CO_2 frequency response was found to be un-attenuated at frequencies ≤ 1 Hz under all RH conditions. A difference between the frequency response under heated and un-heated conditions appeared only for RH > 60 % and was not systematic (data not shown). The corresponding NEON requirement (NEON.TIS.4.1626) was thus fulfilled for CO_2.

In order to further investigate the impact of relative humidity on frequency response, we determined the half-power frequencies as described in Sect. 2.2.3 individually for each half-hour period. The results for the different GSSs and heating strategies are shown in Fig. 7 as a function of relative humidity. In general, 4 W of heating increased $f_{50\,\%}$ by 0.5–1 Hz. For $RH_a < 40$ %, the heated GSS with LN rain cap yielded $f_{50\,\%} > 3$ Hz, approaching the laboratory results of $f_{50\,\%} > 4$ Hz. At higher relative humidities,

AMTD
8, 10983–11028, 2015

the heated GSS with LO rain cap outperformed the heated GSS with LN rain cap, contradicting our laboratory findings.

Together with the change from the LO to the LN rain cap, however, also the intake tube length was changed from 70 to 80 cm, and the ID from 4.8 to 5.3 mm. For the given flow rate set point of 10.8 SL min^{-1} (or ≈ 16.2 L min^{-1} at site conditions), this lead to a reduction of the Reynolds number in the tube of −9.4 % from Re ≈ 3470 to Re ≈ 3150. Following Eq. (11) the half-power frequency of the tube was thus reduced by −32.9 % from 17.1 to 11.5 Hz. For the given volumetric flow rate, the LI-7200 cell by itself yielded $f_{50\,\%}$ = 7.5 Hz due to volume averaging in Eq. (1). Combining LI-7200 cell and the tube according to Eqs. (7)–(10) yielded a half-power frequency reduction of −30.8 % from 6.5 to 4.5 Hz due to the change in intake tube. This effect alone approximately offsets the gain in half-power frequency for changing from LO to LN rain cap as observed in the laboratory (Table 3, from 2.0 Hz to 4.3–6.1 Hz). In addition, not only did the tube inner volume increase by 42 % from 12.4 to 17.7 cm^3, but also the inner surface area increased by 28 % from 104.5 to 133.2 cm^2. As a result, the surface heating from the heater into the tube effectively decreased from 363.8 ± 19.1 W m^{-2} to 307.8 ± 52.6 W m^{-2}. The combined effects resulting from changes in the tube ID and length increased the residence time in the tube, decreased turbulence in the tube, promoted surface adsorption of H_2O, and thus reduced the frequency response in particular under high relative humidity conditions. This explains that for a given 4 W heater setting, the GSS with LN rain cap performs similar to the GSS with LO rain cap for $RH_a < 60\,\%$, but performs worse for $RH_a > 60\,\%$. It should also be mentioned that the final NEON design uses a flow rate of 11.8 SL min^{-1} across sites, thus promoting turbulence development in the intake tube in excess of the setup studied here.

Applying Eqs. (7)–(10) to the half-power frequencies for the LI-7200 ($f_{50\,\%}$ = 7.5 Hz), 80 cm tube with 5.3 mm ID ($f_{50\,\%}$ = 11.5 Hz), filter FW-2.0 ($f_{50\,\%}$ = 17.4 Hz) and LN rain cap ($f_{50\,\%}$ = 12.05 Hz) yielded a system half-power frequency of $f_{50\,\%}$ = 3.1 Hz. This matched the field results in Fig. 7 at 35 % relative humidity. Substituting in Eqs. (7)–(10) the 80 cm tube with 5.3 mm ID by the 70 cm tube with 4.8 mm ID ($f_{50\,\%}$ = 17.1 Hz), the half-power frequency for a virtually improved system was estimated to $f_{50\,\%} = 3.9$ Hz at 35 % relative humidity. The average decrease of $\Delta f_{50\,\%} = 0.36$ Hz per 10 % RH for the observed heated GSS with LO rain cap was utilized to extrapolate $f_{50\,\%} = 2.1$ Hz for the improved system at 85 % relative humidity. This compares to the observed $f_{50\,\%} = 0.6$ Hz and $f_{50\,\%} = 0.9$ Hz for the heated GSS with LN and LO rain caps, respectively. Using Eq. (6), the signal attenuation at 1 Hz for $RH_a = 85\,\%$ can now be determined to 74, 55 and 19 % for the original heated GSS with LO and LN rain cap, and the improved GSS, respectively. While even the improved GSS is not fulfilling the corresponding NEON requirement (NEON.TIS.4.1626), attenuation rapidly decreased to < 5 % at 0.5 Hz. This still warrants the application of automated spectral correction procedures (e.g., Nordbo and Katul, 2012) for NEON towers with a minimum measurement height of 6 m, which was the objective underlying the requirement. Moreover, for passive, first-order low-pass filter systems, the use of resistor-capacitor theory was found to be a convenient alternative to a full convolution of all transfer functions: the knowledge of a single parameter, the half-power frequency, is sufficient to propagate and combine results, which should also be useful for other studies.

Ultimately, the GSS optimization aims at minimizing the need for cospectral correction of the EC fluxes. We found that for the unheated GSS with LO rain cap, the H_2O correction is in excess of 5 % for $RH_a > 60\,\%$, and that 4 W of heating reduces the cospectral correction by almost a similar amount (data not shown). For the GSS with LN rain cap and 4 W of heating, the cospectral correction never exceeded ≈ 3 %, even at very high relative humidity. For CO_2, heated and unheated GSS with LO rain caps required marginal co-spectral corrections, while practically no co-spectral correction was required for the heated GSS with LN rain cap. This further confounds the interpretation of LN high-frequency response gains being offset for H_2O by intensified tube wall effects due to longer and larger ID tubing.

At the given measurement height of 13.7 m above displacement height, the amplitude of fluctuations at frequencies > 1 Hz can approach the detection limit of an enclosed IRGA, in our study resulting in 19 % data loss (Sect. 2.2.3). In addition, the

AMTD
8, 10983–11028, 2015

July 2014 period (LN rain cap) was drier than the July 2013 period (LO rain cap), but also the H_2O fluctuations and flux were $\approx 1/3$ lower in 2014 compared to 2013 (not shown). As a result, the July 2014 power spectra began to display noise at lower frequencies. This also moves the minimum of the transfer function, and hence the base for calculating the half-power frequencies, towards lower frequencies for the GSS with the LN rain cap. Consequently, by measuring closer to the ground with more energy contained in small eddies, as well as operating the different GSSs simultaneously, it should be possible to further improve the field intercomparison.

4 Summary and conclusions

We have shown that a re-examination of the gas analyser sampling system (intake tube, particulate filter, rain cap) can improve practicability and frequency response for eddy-covariance applications. Specifically, overall maintenance, pressure drop and pump and power dimensioning, as well as high-frequency attenuation can all be reduced substantially. Every closed-path or enclosed gas analyser relies on at least some of these gas sampling components, and this study determined their relative importance and provided practical design suggestions. In summary, a rain cap with a minimum volume, 2 µm pleated mesh particulate filter, 70 cm long stainless steel tube with 4.8 mm inner diameter and 4 W of filter and tube heating provided a robust design compromise permitting more automated and scalable operation and data processing

To our knowledge, this is the first study to show that large rain caps can limit overall system frequency response. A redesign can yield up to six-fold improvements, and small volume ($\leq 3\,cm^3$) rain caps thus provide a suitable compromise between water ingress protection and spectral quality. Next, it was shown that the filter choice can result in three orders of magnitude differences in pressure drop, and one order of magnitude difference in frequency response. A 2 µm pleated mesh filter was found to provide the most suitable trade-off between protection from dirt accumulating in the gas analyser, power demand and spectral quality. The selected short and thin intake tube

AMTD
8, 10983–11028, 2015

was found to not limit frequency response. However, a 10 % increase in the tube length and inner diameter resulted in a 1/3 decrease in frequency response, effectively limiting the system. This was attributed to the reduction in surface heating and Reynolds number at given heater and flow rate settings, respectively. Heating the intake tube and particulate filter continuously with 4 W was found to improve the detectability of high-frequency H_2O fluctuations, and no further improvement was found for higher heating powers.

The National Ecological Observatory Network (NEON) has adopted a requirements-based approach for allowing its scientific infrastructure to address interactions of ecosystems, climate, and land use at pre-defined uncertainty levels. Here, this integrative strategy was applied to the development of an infrared gas analyser system for eddy-covariance applications. In this process, all but two of the corresponding technical requirements were fulfilled: (i) None of the tested heater settings were capable of continuously decreasing the relative humidity to $\leq 60\,\%$ in the gas analyser, and (ii) for high relative humidity levels the H_2O system response at 1 Hz was attenuated by up to 19 %. However, it was shown that the objective underlying these requirements can be accomplished, i.e. the application of adaptive correction procedures and automated data processing across field sites. This is a fundamental prerequisite for emergent environmental observatories such as NEON and the Integrated Carbon Observing System (ICOS): advancing ecological inference from local to continental scales rests on the shoulders of an integrated, unbiased, highly scalable and robust combination of instruments and data processing across eco-climatic zones.

Data availability

We provide an external supplement (see https://w3id.org/smetzger/Metzger-et-al_2015_IRGA-GSS) including (i) an extended abstract, (ii) a complete list of NEON requirements regarding dimensioning of the infrared gas analyser and its gas sampling system, (iii) a dimensional drawing of the NEON rain cap, as well as (iv) all NEON raw data used in this study accompanied by variable documentation.

AMTD
8, 10983–11028, 2015

Acknowledgements. We are thankful to Tyler Anderson, Mark Johnson, Mike Furtaw, Jess Raw, Dan Konz, Bob Eckles, and Adam Krueger at LI-COR Biosciences for performing many of the laboratory tests from 2008 to 2014. Many colleagues at the National Ecological Observatory Network supported this study. In particular, Theodore Hehn designed the NEON rain cap, Doug Kath performed the majority of the laboratory tests, Janae Csavina, Ben Duval and Mike Stewart commented on an earlier version of the manuscript, and Jeffrey Taylor (now: Aspen Global Change Institute), Andrea Thorpe and Russ Lea helped shepherding this study and its publication through required administrative procedures. The National Ecological Observatory Network is a project solely sponsored by the National Science Foundation and managed under cooperative agreement by NEON, Inc. This material is based upon work supported by the National Science Foundation under Cooperative Service Agreement EF-1029808. Any opinions, findings, and conclusions or recommendations expressed in this material are those of the author(s) and do not necessarily reflect the views of the National Science Foundation. Mention of a commercial company or product does not constitute an endorsement by the National Ecological Observatory Network or by the National Science Foundation. The US-NR1 AmeriFlux site is currently supported by the United States Department of Energy, Office of Science through the AmeriFlux Management Project at Lawrence Berkeley National Laboratory under Award Number 7094866.

References

Ammann, C., Brunner, A., Spirig, C., and Neftel, A.: Technical note: Water vapour concentration and flux measurements with PTR-MS, Atmos. Chem. Phys., 6, 4643–4651, doi:10.5194/acp-6-4643-2006, 2006.

Aubinet, M., Vesala, T., and Papale, D., (Eds.): Eddy Covariance: A Practical Guide to Measurement and Data Analysis, Springer, Dordrecht, Heidelberg, London, New York, 438 pp., 2012.

Baldocchi, D. D., Hincks, B. B., and Meyers, T. P.: Measuring biosphere–atmosphere exchanges of biologically related gases with micrometeorological methods, Ecology, 69, 1331–1340, doi:10.2307/1941631, 1988.

Brock, F. V.: A nonlinear filter to remove impulse noise from meteorological data, J. Atmos. Ocean. Tech., 3, 51–58, doi:10.1175/1520-0426(1986)003<0051:anftri>2.0.co;2, 1986.

AMTD

8, 10983–11028, 2015

Optimization of a gas sampling system for measuring eddy-covariance fluxes

S. Metzger et al.

Burba, G., McDermitt, D. K., Anderson, D. J., Furtaw, M. D., and Eckles, R. D.: Novel design of an enclosed CO_2/H_2O gas analyser for eddy covariance flux measurements, Tellus B, 62, 743–748, doi:10.1111/j.1600-0889.2010.00468.x, 2010.

Burba, G., Schmidt, A., Scott, R. L., Nakai, T., Kathilankal, J., Fratini, G., Hanson, C., Law, B., McDermitt, D. K., Eckles, R., Furtaw, M., and Velgersdyk, M.: Calculating CO_2 and H_2O eddy covariance fluxes from an enclosed gas analyzer using an instantaneous mixing ratio, Glob. Change Biol., 18, 385–399, doi:10.1111/j.1365-2486.2011.02536.x, 2012.

Burns, S. P., Metzger, S., Blanken, P. D., Burba, G., Swiatek, E., Li, J., Conrad, B., Luo, H., and Taylor, J. R.: A comparison of infrared gas analyzers above a subalpine forest in complex terrain, Preprints, 17th Symposium on Meteorological Observation and Instrumentation, Westminster, USA, 9–13 June 2014, 13, 2014.

Clement, R. J., Burba, G. G., Grelle, A., Anderson, D. J., and Moncrieff, J. B.: Improved trace gas flux estimation through IRGA sampling optimization, Agr. Forest Meteorol., 149, 623–638, doi:10.1016/j.agrformet.2008.10.008, 2009.

De Ligne, A., Joly, L., Chopin, H., Cousin, J., Chauvin, N., Decarpenterie, T., and Aubinet, M.: Laboratory and field experiments in order to dimension the IRGA gas sampling system, 1st ICOS Science Conference on Greenhouse Gases and Biogeochemical Cycles, Brussels, Belgium, 23–25 September 2014, 27, 2014.

Eugster, W. and Senn, W.: A cospectral correction model for measurement of turbulent NO_2 flux, Boundary Lay. Meteorol., 74, 321–340, doi:10.1007/bf00712375, 1995.

Foken, T., Leuning, R., Oncley, S. P., Mauder, M., and Aubinet, M.: Corrections and data quality control, in: Eddy covariance: A Practical Guide to Measurement and Data Analysis, edited by: Aubinet, M., Vesala, T., and Papale, D., Springer, Dordrecht, Heidelberg, London, New York, 85–131, 2012.

Fratini, G., Ibrom, A., Arriga, N., Burba, G., and Papale, D.: Relative humidity effects on water vapour fluxes measured with closed-path eddy-covariance systems with short sampling lines, Agr. Forest Meteorol., 165, 53–63, doi:10.1016/j.agrformet.2012.05.018, 2012.

Fratini, G., McDermitt, D. K., and Papale, D.: Eddy-covariance flux errors due to biases in gas concentration measurements: origins, quantification and correction, Biogeosciences, 11, 1037–1051, doi:10.5194/bg-11-1037-2014, 2014.

Ibrom, A., Dellwik, E., Flyvbjerg, H., Jensen, N. O., and Pilegaard, K.: Strong low-pass filtering effects on water vapour flux measurements with closed-path eddy correlation systems, Agr. Forest Meteorol., 147, 140–156, doi:10.1016/j.agrformet.2007.07.007, 2007.

AMTD

8, 10983–11028, 2015

Kaimal, J. C., Wyngaard, J. C., Izumi, Y., and Coté, O. R.: Spectral characteristics of surface-layer turbulence, Q. J. Roy. Meteor. Soc., 98, 563–589, doi:10.1002/qj.49709841707, 1972.
Lee, G. Y. and Gill, W. N.: A note on velocity and eddy viscosity distributions in turbulent shear flows with free surfaces, Chem. Eng. Sci., 32, 967–969, doi:10.1016/0009-2509(77)80083-3, 1977.
Lee, G. Y. and Gill, W. N.: Dispersion in turbulent film flow, Chem. Eng. Commun., 4, 607–641, doi:10.1080/00986448008935935, 1980.
Lenschow, D. and Sun, J.: The spectral composition of fluxes and variances over land and sea out to the mesoscale, Boundary Lay. Meteorol., 125, 63–84, doi:10.1007/s10546-007-9191-8, 2007.
Lubchenco, J., Olson, A. M., Brubaker, L. B., Carpenter, S. R., Holland, M. M., Hubbell, S. P., Simon, A. L., MacMahon, J. A., Matson, P. A., Melillo, J. M., Mooney, H. A., Peterson, C. H., Pulliam, H. R., Real, L. A., Regal, P. J., and Risser, P. G.: The sustainable biosphere initiative: an ecological research agenda: a report from the ecological society of america, Ecology, 72, 371–412, doi:10.2307/2937183, 1991.
Massman, W. J.: The attenuation of concentration fluctuations in turbulent flow through a tube, J. Geophys. Res.-Atmos., 96, 15269–15273, doi:10.1029/91jd01514, 1991.
Massman, W. J.: Concerning the measurement of atmospheric trace gas fluxes with open- and closed-path eddy covariance system: The WPL terms and spectral attenuation, in: Handbook of Micrometeorology: A Guide for Surface Flux Measurement and Analysis, 1 edn., edited by: Lee, X., Law, B., and Massman, W., Springer, Dordrecht, 67–100, 2004.
Massman, W. J. and Ibrom, A.: Attenuation of concentration fluctuations of water vapor and other trace gases in turbulent tube flow, Atmos. Chem. Phys., 8, 6245–6259, doi:10.5194/acp-8-6245-2008, 2008.
Mauder, M. and Foken, T.: Documentation and instruction manual of the eddy-covariance software package TK3, Arbeitsergenisse Abteilung Mikrometeorologie, 46, Universität Bayreuth, Bayreuth, Germany, 60 pp., ISSN 1614–8924, 2011.
Metzger, S., Junkermann, W., Mauder, M., Beyrich, F., Butterbach-Bahl, K., Schmid, H. P., and Foken, T.: Eddy-covariance flux measurements with a weight-shift microlight aircraft, Atmos. Meas. Tech., 5, 1699–1717, doi:10.5194/amt-5-1699-2012, 2012.
Metzger, S., Junkermann, W., Mauder, M., Butterbach-Bahl, K., Trancón y Widemann, B., Neidl, F., Schäfer, K., Wieneke, S., Zheng, X. H., Schmid, H. P., and Foken, T.: Spatially

explicit regionalization of airborne flux measurements using environmental response functions, Biogeosciences, 10, 2193–2217, doi:10.5194/bg-10-2193-2013, 2013.
Metzger, S., Burns, S. P., Luo, H., Hehn, T., Kath, D., Burba, G., Li, J., Anderson, T., Blanken, P. D., and Taylor, J. R.: A gas analyzer sampling system optimized for eddy-covariance applications, 17th Symposium on Meteorological Observation and Instrumentation, Westminster, USA, 9–13 June 2014, 3, 2014.
Moncrieff, J. B., Massheder, J. M., de Bruin, H., Elbers, J., Friborg, T., Heusinkveld, B., Kabat, P., Scott, S., Soegaard, H., and Verhoef, A.: A system to measure surface fluxes of momentum, sensible heat, water vapour and carbon dioxide, J. Hydrol., 188–189, 589–611, doi:10.1016/S0022-1694(96)03194-0, 1997.
Monson, R. K., Turnipseed, A. A., Sparks, J. P., Harley, P. C., Scott-Denton, L. E., Sparks, K., and Huxman, T. E.: Carbon sequestration in a high-elevation, subalpine forest, Glob. Change Biol., 8, 459–478, doi:10.1046/j.1365-2486.2002.00480.x, 2002.
Monson, R. K., Prater, M. R., Hu, J., Burns, S. P., Sparks, J. P., Sparks, K. L., and Scott-Denton, L. E.: Tree species effects on ecosystem water-use efficiency in a high-elevation, subalpine forest, Oecologia, 162, 491–504, doi:10.1007/s00442-009-1465-z, 2010.
Moore, C. J.: Frequency-response corrections for eddy-correlation systems, Boundary Lay. Meteorol., 37, 17–35, doi:10.1007/BF00122754, 1986.
National Research Council: Grand Challenges in Environmental Sciences, The National Academies Press, Washington, DC, 96 pp., 2001.
Nordbo, A. and Katul, G.: A wavelet-based correction method for eddy-covariance high-frequency losses in scalar concentration measurements, Boundary Lay. Meteorol., 146, 81–102, doi:10.1007/s10546-012-9759-9, 2012.
Philip, J. R.: The damping of a fluctuating concentration by continuous sampling through a tube, Aust. J. Phys., 16, 454–463, doi:10.1071/PH630454, 1963.
R Development Core Team: R: A language and environment for statistical computing, R Foundation for Statistical Computing, Vienna, Austria, 2012.
Rannik, Ü., Vesala, T., and Keskinen, R.: On the damping of temperature fluctuations in a circular tube relevant to the eddy covariance measurement technique, J. Geophys. Res.-Atmos., 102, 12789–12794, doi:10.1029/97jd00362, 1997.
Runkle, B., Wille, C., Gažovič, M., and Kutzbach, L.: Attenuation correction procedures for water vapour fluxes from closed-path eddy-covariance systems, Boundary Lay. Meteorol., 142, 401–423, doi:10.1007/s10546-011-9689-y, 2012.

Schimel, D., Keller, M., Berukoff, S., Kao, B., Loescher, H., Powell, H., Kampe, T., Moore, D., Gram, W., Barnett, D., Gallery, R., Gibson, C., Goodman, K., Meier, C., Parker, S., Pitelka, L., Springer, Y., Thibault, K., and Utz, R.: Science Strategy – Enabling Continental-Scale Ecological Forecasting, National Ecological Observatory Network, Boulder, USA, 56 pp., 2011.
Silverman, B. A.: The effect of spatial averaging on spectrum estimation, J. Appl. Meteorol., 7, 168–172, doi:10.1175/1520-0450(1968)007<0168:teosao>2.0.co;2, 1968.
Swinbank, W. C.: The measurement of vertical transfer of heat and water vapor by eddies in the lower atmosphere, J. Meteorol., 8, 135–145, doi:10.1175/1520-0469(1951)008<0135:tmovto>2.0.co;2, 1951.
Truax, B.: Handbook for Acoustic Ecology, originally published by: The World Soundscape Project, Simon Fraser University, and ARC Publications, 1978, Cambridge Street Publishing, Burnaby, Canada, 160 pp., 1999.
Turnipseed, A. A., Blanken, P. D., Anderson, D. E., and Monson, R. K.: Energy budget above a high-elevation subalpine forest in complex topography, Agr. Forest Meteorol., 110, 177–201, doi:10.1016/S0168-1923(01)00290-8, 2002.
Turnipseed, A. A., Anderson, D. E., Blanken, P. D., Baugh, W. M., and Monson, R. K.: Airflows and turbulent flux measurements in mountainous terrain: Part 1. Canopy and local effects, Agr. Forest Meteorol., 119, 1–21, doi:10.1016/s0168-1923(03)00136-9, 2003.
Webb, E. K., Pearman, G. I., and Leuning, R.: Correction of flux measurements for density effects due to heat and water vapour transfer, Q. J. Roy. Meteor. Soc., 106, 85–100, doi:10.1002/qj.49710644707, 1980.
Wilczak, J. M., Oncley, S. P., and Stage, S. A.: Sonic anemometer tilt correction algorithms, Boundary Lay. Meteorol., 99, 127–150, doi:10.1023/A:1018966204465, 2001.
Williams, A. and Taylor, F. J.: Electronic Filter Design Handbook, 4th edn., McGraw-Hill, New York, USA, 775 pp., 2006.

AMTD
8, 10983–11028, 2015

Table 1. Candidate filters and filter materials considered in this study, and their key characteristics including pore size (pore), length (d_l) and inner diameter (d_{id}).

Manufacturer	Filter model	Material	Pore [µm]	d_l [mm]	d_{id} [mm]	Abbreviation
3M/CUNO, Meriden, CT, USA	PolyPro XL G250 filter capsule	polypropylene housing and membrane	2.5	50.8	7.0	PP-2.5
3M/CUNO, Meriden, CT, USA	PolyPro XL G500 filter capsule	polypropylene housing and membrane	5.0	50.8	7.0	PP-5.0
Advantec MFS, Dublin, CA, USA	LS 25	stainless steel housing and nylon membrane	1.2	50.0	38.0	LS25-1.2
Advantec MFS, Dublin, CA, USA	LS 25	stainless steel housing and nylon membrane	5.0	50.0	38.0	LS25-5.0
Advantec MFS, Dublin, CA, USA	LS 47	stainless steel housing and nylon membrane	5.0	57.0	69.0	LS47-5.0
Pall Corporation, Port Washington, NY, USA	Acro 50	polypropylene housing and polytetrafluoroethylene (PTFE) membrane	1.0	82.0	73.0	AC-1.0
Swagelok, Solon, OH, USA	F-series	stainless steel housing and sintered stainless steel element	2.0	54.6	4.8	F-2.0
Swagelok, Solon, OH, USA	FW-series	stainless steel housing and pleated stainless steel mesh	2.0	54.6	4.8	FW-2.0
ZenPure, Manassas, VA, USA	PureFlo PTFE filter capsule	polypropylene housing and polytetrafluoroethylene (PTFE) membrane	0.1	127.0	73.0	PF-0.1

AMTD
8, 10983–11028, 2015

Table 2. Components tested in detail in the laboratory and field experiments including LI-COR old (LO), LI-COR new (LN) and NEON new (NN) rain caps, and the Swagelok FW-2.0 filter (Table 1 provides detailed specifications). Key characteristics include length (d_l), inner diameter (d_{id}), outer diameter (d_{od}) and volume (V). Only components and materials selected for this study are shown, and numerous alternatives are excluded. Cross combinations were also tested.

Component	d_l [mm]	d_{id} [mm]	d_{od} [mm]	V [cm^3]
laboratory and field tests				
rain cap LO	17.5	36.0	41.9	17.8
rain cap LN	11.4	19.1	25.4	3.2
filter FW-2.0	54.6	4.8	25.4	1.0
sampling cell LI-7200	125.0	12.8	75.0	16.0
laboratory tests only				
rain cap NN	50.8	6.4–17.8	50.8	2.4
intake tube	700.0–1016.0	4.8–5.3	6.4	12.4–22.6
field tests only				
intake tube for rain cap LO	700.0	4.8	6.4	12.4
intake tube for rain cap LN	800.0	5.3	6.4	17.7

AMTD
8, 10983–11028, 2015

Table 3. CO_2 and H_2O half-power frequencies for system components without heating or insulation, for the range of flow rates 9.5 to 14 SLPM, as derived from the data shown in Figs. 2–3. Ranges from multiple experiments are provided when available. Rain caps are NEON new (NN), LI-COR new (LN) and LI-COR old (LO). Filters are Swagelok FW-2.0, 3M/CUNO PP-2.5, 3M/CUNO PP-5.0, Pall AC-1.0 and ZenPure PF-0.1 (Table 1 provides detailed filter specifications).

System elements	CO_2	H_2O
rain cap NN	16.5 Hz	14.3 Hz
rain cap LN	12.3–13.8 Hz	11.8–12.3 Hz
rain cap LO	2.5 Hz	2.4 Hz
filter FW-2.0	16.4–16.5 Hz	14.9–19.9 Hz
filter PP-2.5	21.8 Hz	5.4–7.0 Hz
filter PP-5.0	18.9 Hz	5.0–8.8 Hz
filter AC-1.0	18.7 Hz	2.2–3.9 Hz
filter PF-0.1	8.3 Hz	1.4–4.0 Hz
intake tube (d_l = 700 mm, d_{id} = 4.8 mm)	19.9 Hz	15.9 Hz
intake tube + rain cap NN	11.9 Hz	9.8 Hz
intake tube + rain cap LN	9.7–14.6 Hz	5.9–9.6 Hz
intake tube + rain cap LO	2.2 Hz	1.9 Hz
intake tube + filter FW-2.0	11.9–15.4 Hz	11.2–11.6 Hz
intake tube + filter FW-2.0 + rain cap NN	12.0 Hz	9.3 Hz
intake tube + filter FW-2.0 + rain cap LN	5.3–10.2 Hz	4.3–6.1 Hz
intake tube + filter FW-2.0 + rain cap LO	2.2 Hz	2.0 Hz

Discussion Paper | Discussion Paper | Discussion Paper | Discussion Paper |

AMTD

8, 10983–11028, 2015

Optimization of a gas sampling system for measuring eddy-covariance fluxes

S. Metzger et al.

Title Page
Abstract Introduction
Conclusions References
Tables Figures
◂◂ ▸▸
◂ ▸
Back Close
Full Screen / Esc
Printer-friendly Version
Interactive Discussion

AMTD
8, 10983–11028, 2015

Table 4. Descriptive statistics (median and median absolute deviation) covering periods of different heating settings of the LI-7200 intake tube and filter. The header distinguishes combinations of different rain caps (LO, LN) and heater settings (0 Watt, 4 Watt, 5 Watt, 6 Watt). Shown are ambient temperature (T_a), LI-7200 inlet temperature (T_{in}), LI-7200 outlet temperature (T_{out}), LI-7200 block temperature (T_{block}), ambient relative humidity (RH_a) and LI-7200 cell relative humidity (RH_{cell}).

Variable	LO-0 Watt	LO-4 Watt	LN-4 Watt	LO-5 Watt	LO-6 Watt
begin date	6 Jul 2013	2 Jul 2013	1 Jul 2014	11 Jul 2013	23 Jul 2013
end date	11 Jul 2013	6 Jul 2013	9 Jul 2014	23 Jul 2013	31 Jul 2013
heating power [W]	0.0 ± 0.0	3.8 ± 0.2	4.1 ± 0.7	5.4 ± 0.2	6.3 ± 0.1
T_a [°C]	15.1 ± 2.9	11.7 ± 3.0	12.8 ± 3.7	14.4 ± 3.2	11.8 ± 2.7
$T_{in} - T_a$ [°C]	0.2 ± 1.0	6.7 ± 0.7	7.7 ± 1.6	9.6 ± 0.9	12.7 ± 1.0
$T_{in} - T_{out}$ [°C]	-0.1 ± 0.2	3.7 ± 0.2	4.0 ± 0.9	5.5 ± 0.3	6.9 ± 0.2
$T_{in} - T_{block}$ [°C]	-0.3 ± 0.2	5.7 ± 0.3	6.0 ± 1.4	8.4 ± 0.5	10.6 ± 0.4
RH_a [%]	46.1 ± 10.8	63.1 ± 14.6	50.0 ± 20.9	55.5 ± 29.6	68.7 ± 17.8
RH_{cell} [%]	44.7 ± 12.2	48.7 ± 13.7	39.0 ± 15.2	38.5 ± 20.9	41.7 ± 11.3
$RH_a - RH_{cell}$ [%]	1.0 ± 2.9	14.9 ± 1.9	11.6 ± 4.8	16.2 ± 8.2	24.7 ± 7.2
sample size (half-hours)	190	183	284	288	275

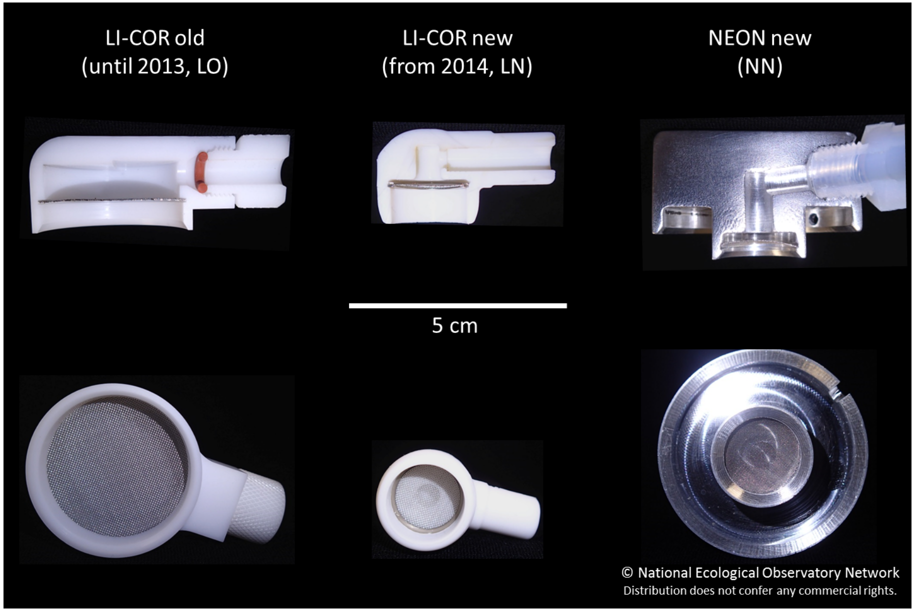

Figure 1. Three selected rain cap designs tested in this study. Top row: cross-sections of each rain cap showing their internal volumes. Bottom row: rain cap inlets with screens that face downwards in typical field deployments.

AMTD
8, 10983–11028, 2015

Optimization of a gas sampling system for measuring eddy-covariance fluxes

S. Metzger et al.

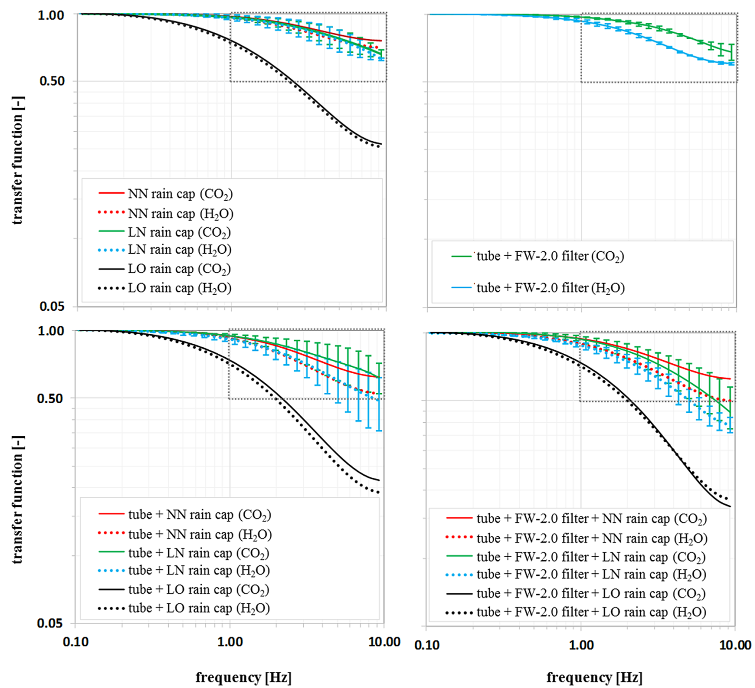

Figure 2. Transfer functions of different gas sampling system components and combinations thereof, without heating or insulation. Dotted grey boxes indicate approximate desirable ranges for a short-tube low-power implementation, requiring minimal corrections. Bars indicate range from multiple experiments, where available, as described in Sect. 2.1. Please note that the *y* axis starts at 0.05. Top left panel: three selected rain caps NEON new (NN), LI-COR new (LN) and LI-COR old (LO), without tube and filter. Top right panel: tube and Swagelok FW-2.0 filter (Table 1 provides detailed specifications), without rain cap. Bottom left panel: tube and three selected rain caps, without filter. Bottom right panel: tube, FW-2.0 filter and three selected rain caps.

AMTD
8, 10983–11028, 2015

Optimization of a gas sampling system for measuring eddy-covariance fluxes

S. Metzger et al.

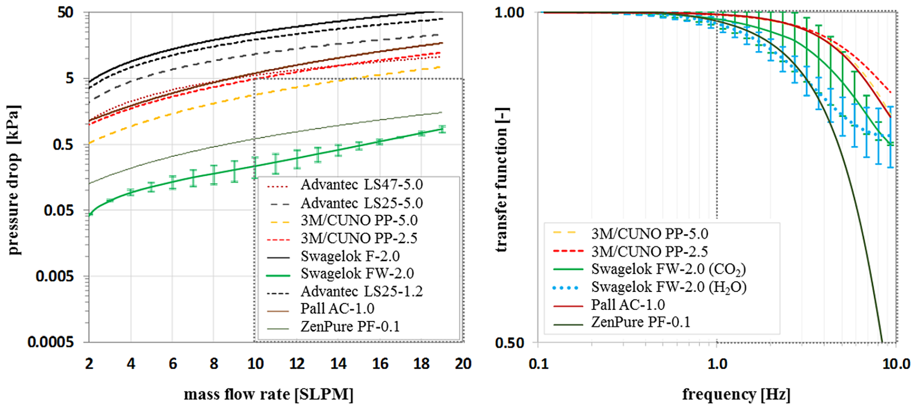

Figure 3. Optimization of an intake particulate filter. Dotted grey boxes indicate approximate desirable ranges for a short-tube low-power implementation, requiring minimal corrections. Left panel: pressure drop of nine tested filters at different flow rates, without tube and rain cap (Table 1 provides detailed filter specifications). Please note the log-scale of *y* axis. Right panel: transfer function of five selected filters, without tube, rain cap, heating or insulation. Please note that *y* axis starts at 0.5. Bars indicate range from multiple experiments, where available, as described in Sect. 2.1.

AMTD
8, 10983–11028, 2015

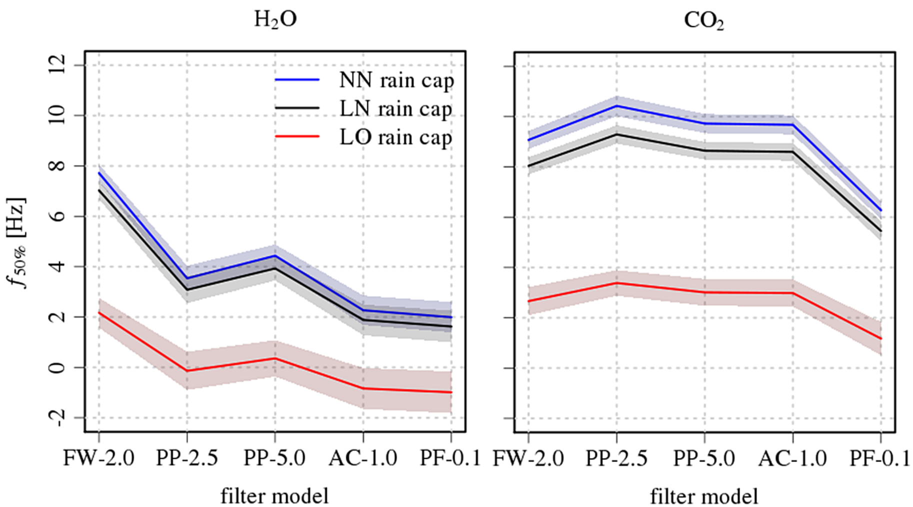

Figure 4. Half-power frequencies of filter and rain cap combinations without tube for H_2O (left panel) and CO_2 (right panel). Rain caps are NEON new (NN), LI-COR new (LN) and LI-COR old (LO). Filters are Swagelok FW-2.0, 3M/CUNO PP-2.5, 3M/CUNO PP-5.0, Pall AC-1.0 and ZenPure PF-0.1 (Table 1 provides detailed filter specifications). Values are determined by propagating combinations of individual filter and rain cap half-power frequencies (Table 3) through Eqs. (7)–(10). The shaded areas represent the standard error resulting from regression Eq. (7).

AMTD
8, 10983–11028, 2015

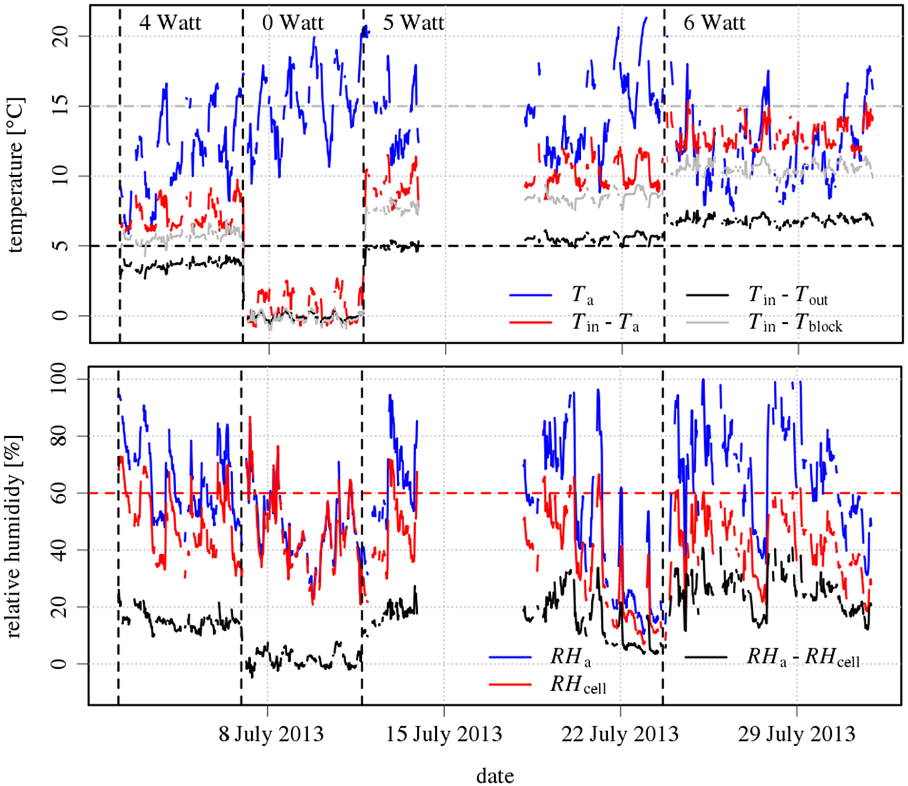

Figure 5. Example time series of the ambient air temperature and relative humidity during periods of different heating settings of the LI-7200 intake tube and filter, indicated by the dashed vertical lines. Top panel: ambient air temperature (T_a), LI-7200 cell inlet, outlet and block temperature (T_{in}, T_{out}, T_{block}, respectively) and differences thereof. The dashed horizontal line indicates a 5 °C threshold for the temperature gradient across the LI-7200 cell. Bottom panel: ambient relative humidity (RH_a), in the LI-7200 cell (RH_{cell}), and differences thereof.

AMTD
8, 10983–11028, 2015

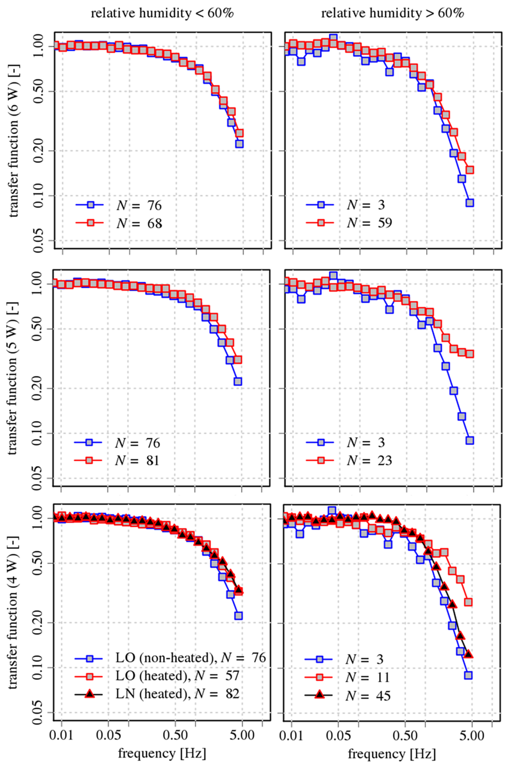

Figure 6. Ensemble transfer functions of LI-7200-measured H_2O number density relative to LI-7500 for different heater settings of the intake tube and filter (rows) and ambient relative humidity classes (columns). Shown are results for the LI-COR old (LO) rain cap with and without heating of filter and intake tube, as well as for the LI-COR new (LN) rain cap for the 4 W heater setting, together with the respective ensemble sample size (N). Only half-hours with sensible heat flux > $50\,\mathrm{W\,m^{-2}}$ are used to homogenize the sample size across different test periods.

AMTD
8, 10983–11028, 2015

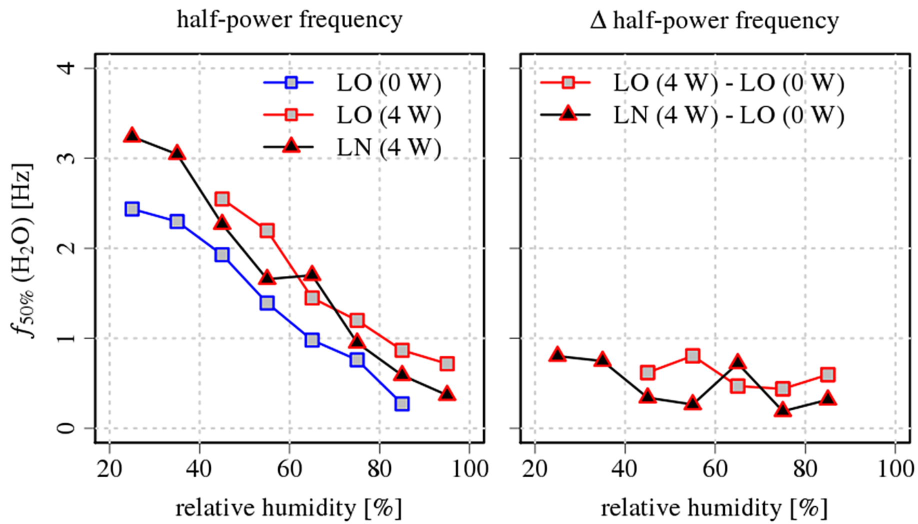

Figure 7. Ensemble half-power frequencies of LI-7200-measured H_2O number density relative to LI-7500 as function of ambient relative humidity. Relative humidity classes without ensemble member are omitted. Left panel: results for the LI-COR old (LO) rain cap without heating of filter and intake tube, as well as the LO and LI-COR new (LN) rain caps for the 4 W heater setting. Right panel: differences in half-power frequency between LO and LN rain caps with 4 W heating of filter and intake tube, and the LO rain cap without heating of filter and intake tube.